ISSN (Print) 1226-1750
ISSN (Online) 2233-6656
Journal of Magnetics 30(4), 802-809 (2025) https://doi.org/10.4283/JMAG.2025.30.4.802

Optimized CT Image Denoising Method Combining Wavelet Transform and U-Net Model

Chanyoung Park[1] and Byungdu Jo[1,2,3]*

[1]*Department of Multidisciplinary Radiological Science, The Graduate School of Dongseo University, Busan 47011, Republic of Korea*
[2]*Department of Radiological Science, Dongseo University, Busan 47011, Republic of Korea*
[3]*Center for Radiological Environment & Health Science, Dongseo University, Busan 47011, Republic of Korea*

(Received 6 November 2025, Received in final form 4 December 2025, Accepted 5 December 2025)

Low-dose computed tomography (CT) is essential for minimizing patient radiation exposure; however, increased noise often leads to image degradation and may adversely affect diagnostic accuracy. In this study, we propose an optimized CT image restoration method that integrates wavelet transform with the U-Net architecture. The proposed approach decomposes the input image into low- and high-frequency components, selectively removes noise from the high-frequency bands, and reconstructs the image while preserving structural information in the low-frequency bands. The reconstructed components are subsequently refined through the U-Net for final denoising. Performance was quantitatively evaluated using PSNR and SSIM, showing improvements in the average PSNR by 10.3% and average SSIM by 14.7%, respectively, compared to the conventional U-Net. These results demonstrate that the wavelet-based U-Net model offers superior denoising performance while maintaining image resolution and anatomical structure, suggesting it as an effective approach for improving the quality of low-dose CT images.

Keywords : low-dose CT, electromagnetic radiation, denoising, U-Net, wavelet transform, deep learning

1. Introduction

Computed tomography (CT) has become an essential imaging modality in the field of radiological diagnosis due to its high spatial resolution and diagnostic accuracy. It is also widely utilized in routine health examinations [1]. The clinical value of CT imaging lies in its ability to accurately detect lesions and guide appropriate treatment planning. However, with the increasing use of low-dose CT (LDCT) to minimize patient radiation exposure, severe noise is often introduced into the images. This noise degrades image quality and negatively affects diagnostic accuracy and lesion identification [2].

To address this issue, effective denoising techniques are required. In recent years, deep learning-based Artificial Intelligence (AI) technologies have rapidly advanced in the field of medical imaging, drawing attention as novel approaches for image restoration and enhancement [3]. Furthermore, Magnetic Resonance Imaging (MRI), which, unlike CT, does not rely on ionizing electromagnetic radiation but instead utilizes strong magnetic fields and radiofrequency waves, serves as a non-invasive modality that provides superior soft-tissue contrast and complementary diagnostic information to CT [4, 5]. While both imaging modalities possess high diagnostic value, challenges such as radiation exposure in CT and increased noise in LDCT remain to be addressed.

Representative deep learning models applied for CT image denoising include Convolutional Neural Networks (CNNs) and Generative Adversarial Networks (GANs). Among these, the CNN-based U-Net model is the most widely used in the medical image restoration domain [6, 7]. The U-Net adopts an encoder-decoder-based auto-encoder structure optimized for effective feature extraction and restoration, showing excellent performance in CT image denoising [8]. However, most deep learning-based denoising approaches, including the conventional U-Net, are limited in that they may lead to the loss of fine structural details or cause blurring effects in images with complex anatomical structures. Therefore, these limitations highlight the necessity of developing advanced denoising strategies to preserve both visual clarity and anatomical

*Corresponding author: Tel: +82-51-320-4274
e-mail: byungdujo@gdsu.dongseo.ac.kr

fidelity in LDCT imaging.

Recent research has proposed various deep learning-based restoration techniques for CT images, with CNN-based models actively explored due to their advantages in structural preservation. Kang *et al.* [9] attempted to enhance LDCT image quality using a residual learning-based CNN, while Chen *et al.* [10] emphasized natural texture restoration through a GAN-based framework. Additionally, Zhang *et al.* [11] proposed a multi-scale residual learning-based image restoration model utilizing the MA-Net architecture. However, many of these approaches still exhibit limitations such as the loss of fine anatomical structures and blurring, as they focus primarily on noise removal.

To overcome these limitations, this study proposes a novel U-Net-based framework that integrates Wavelet Transform into the network architecture. The wavelet transform decomposes the input image into low- and high-frequency components, allowing for effective preservation of structural information while selectively removing high-frequency noise [12, 13]. The proposed model aims to achieve a balance between denoising performance and anatomical structure preservation by combining the multi-resolution analysis capability of wavelet transform with the strong restoration ability of U-Net. The structure of this paper is as follows: Section 2 describes the overall architecture and algorithms of the proposed wavelet-integrated U-Net model. Section 3 presents the quantitative evaluation results, Section 4 validates the effectiveness of the proposed method through comparative analysis, and Section 5 discusses the conclusions and future research directions.

2. Material and Method

2.1. The Wavelet Transform

The wavelet transform is a technique that decomposes image signals into frequency components, allowing the analysis of local time-frequency characteristics [14, 15]. As shown in Fig. 1, the original image can be decomposed into low-frequency components (structural information) and high-frequency components (edges and noise). In particular, the low-frequency band (LL) contains the major anatomical structures, while the high-frequency bands (LH, HL, HH) include edges, textures, and noise [16].

Wavelet transforms are categorized into Continuous Wavelet Transform (CWT) and Discrete Wavelet Transform (DWT) [17]. CWT continuously transforms signals at various scales and time positions to analyze local frequency characteristics, providing high time-frequency resolution. It is defined as follows (1):

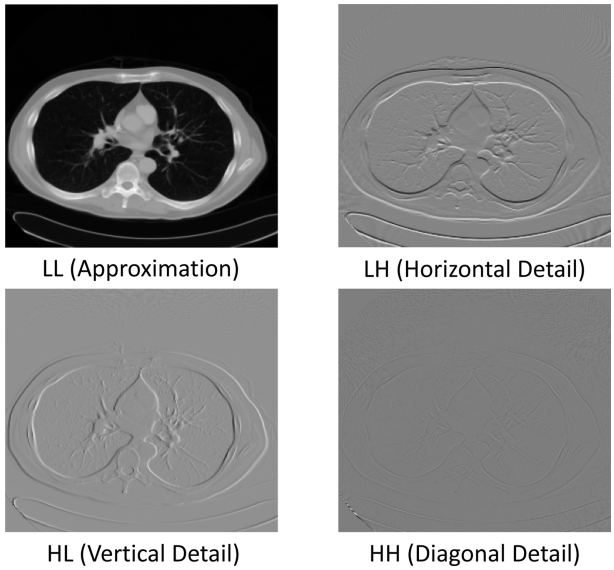

Fig. 1. Wavelet-Decomposed Frequency Components of the CT Image (LL, LH, HL, HH Subbands).

$$\mathrm{CWT}_x(a,b) = \frac{1}{\sqrt{|a|}} \int_{-\infty}^{\infty} x(t)\, \psi^* \left(\frac{t-b}{a} \right) dt \qquad (1)$$

where a is the scale parameter, b is the translation parameter, and ψ^* is the complex conjugate of the mother wavelet. Smaller scales emphasize high-frequency components. CWT provides high time-frequency resolution, but its continuous nature results in high computational complexity, excessive memory usage, and coefficient redundancy [18].

In contrast, DWT limits scale and translation parameters to discrete binary sequences, reducing computational load and improving efficiency. DWT is defined as follows (2):

$$\mathrm{DWT}_x(j,k) = \int x(t) \cdot \psi_{j,k}(t) dt \quad \text{where} \quad \psi_{j,k}(t) = 2^{-\frac{j}{2}} \psi\left(2^{-j}t - k\right) \qquad (2)$$

Here, j and k are the scale and translation parameters, respectively. As the scale increases, time resolution decreases and frequency resolution improves, enabling multi-resolution analysis [19]. Considering both efficiency and precision, DWT was employed in this study to separate CT image signals and selectively remove noise from the high-frequency components.

2.2. Wavelet Mother Function

The Wavelet Mother Function is the foundational function of the wavelet transform, designed to analyze local signal characteristics in the time-frequency domain

[20]. The mother wavelet generates a wavelet family by scaling and translating, allowing comprehensive signal analysis across multiple frequency bands [21].

This study adopts the Daubechies 4 (db4) wavelet function, which has four vanishing moments and eight filter coefficients. Four of these represent low-pass filters for extracting the LL component containing primary structural information, defined as follows (3):

$$h_0 = \frac{1+\sqrt{3}}{4\sqrt{2}},\ h_1 = \frac{3+\sqrt{3}}{4\sqrt{2}},\ h_2 = \frac{3-\sqrt{3}}{4\sqrt{2}},\ h_3 = \frac{1-\sqrt{3}}{4\sqrt{2}} \tag{3}$$

The high-pass filter coefficients are derived from the low-pass coefficients using the following formula (4):

$$g(n) = (-1)^n h(N-1-n) \tag{4}$$

where N is the filter length. The high pass filter effectively extracts edges, textures, and noise in the image. Daubechies wavelets are orthogonal and compactly supported, making them suitable for multi-resolution analysis and efficient in both DWT and inverse DWT [22, 23].

2.3. Wavelet Threshold Factor Setting

After decomposing the image using Wavelet Transform, soft thresholding is applied to the high-frequency components (LH, HL, HH) to selectively remove noise. This method suppresses noise by eliminating small, unnecessary coefficients.

The soft thresholding process is defined by the following equation (5):

$$S_T(x) = \begin{cases} sgn(x)\cdot(|x|-\mathrm{T}), & |x| > \mathrm{T} \\ 0, & |x| \le \mathrm{T} \end{cases} \tag{5}$$

Here, T denotes the threshold value, and coefficients less than or equal to T are removed, while coefficients exceeding T are shrunk by T and preserved. However, to better reflect the local characteristics of the image, this study employed an adaptive thresholding scheme. The threshold value T is generally determined based on statistical characteristics, as shown in the following equation (6):

$$\mathrm{T} = \sigma\sqrt{2\log n} \tag{6}$$

Where σ is the standard deviation of the noise, and n is the number of wavelet coefficients. This approach is designed to exclude the possibility of spuriously large values among numerous coefficients based on probabilistic theory, such as the expected value of the maximum or the probability of maximum noise, thus providing a theoretically universal and automated criterion [24, 25]. However, given the specific nature of medical image processing, an application-specific threshold setting is necessary to reflect data peculiarities, such as visual quality enhancement and noise suppression. Therefore, the threshold value was determined using the following empirical formula (7):

$$\mathrm{T} = \mathrm{k}\cdot\mathrm{w}\cdot\sigma \tag{7}$$

Here, k is the scaling factor, w is the band-level correction factor, and σ is the standard deviation of the noise. This formula allows for dynamic adjustment of the threshold based on the distribution characteristics of the noise and changes in resolution within the image, enabling effective noise suppression while preserving fine details [26].

2.4. Image Segmentation

For quantitative evaluation of denoising performance, this study defined a Region of Interest (ROI) based on automated segmentation of thoracic and abdominal CT images [27-29]. After converting DICOM images to

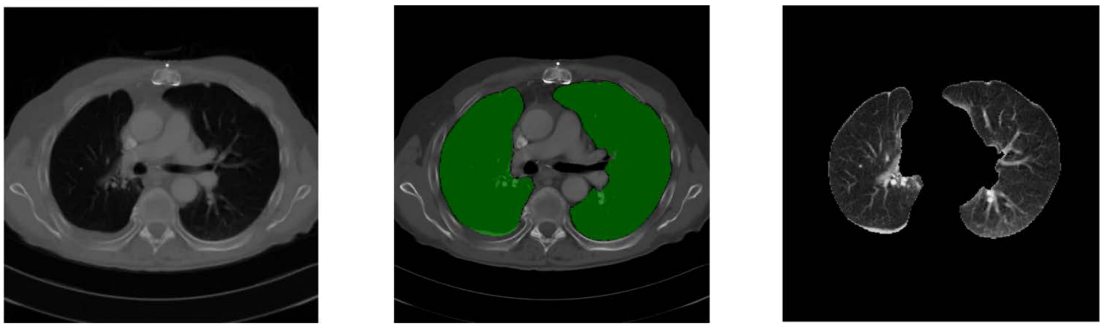

Fig. 2. (Color online) ROI Generation Pipeline for Chest/Abdomen CT Images.

Hounsfield Units (HU), an initial automatic lung mask was generated using the lungmask library. If the lung area was insufficient or absent, an adaptive ROI generation algorithm was applied. This alternative strategy involved considering areas with soft tissue HU values (e.g., -1000 to -400 for lung, or 20 to 70 for other soft tissues) to construct a mask. If all criteria failed, a central soft tissue mask (-300 to 300 HU) covering 20% to 80% of the image was generated. Finally, high-density tissues (bone, HU > 400) were removed, and morphological operations were applied to secure contiguous ROI. The ROI generation process is illustrated in Fig. 2.

2.5. Application of Wavelet Transform

In this study, the Wavelet Transform was applied as a preprocessing step for CT images. As shown in Fig. 3, the process begins by decomposing the image into low-frequency components (representing primary structural information) and high-frequency components (representing boundary details and noise). The low-frequency components are preserved, while the high-frequency components are processed to selectively remove noise while retaining important boundary information. Finally, the low-frequency and denoised high-frequency components are reconstructed into a single image using the Inverse Wavelet Transform (IDWT).

The architecture of the U-Net used in this study is shown in Fig. 4. This reconstructed image is then used as the input (256 × 256 × 1) for the U-Net model. The U-Net consists of an encoding path, a bottleneck layer, and a decoding path. The encoding path uses two convolutional blocks and pooling layers to progressively compress the features and extract high-level representations (32 to 64 channels), halving the spatial resolution. The bottleneck

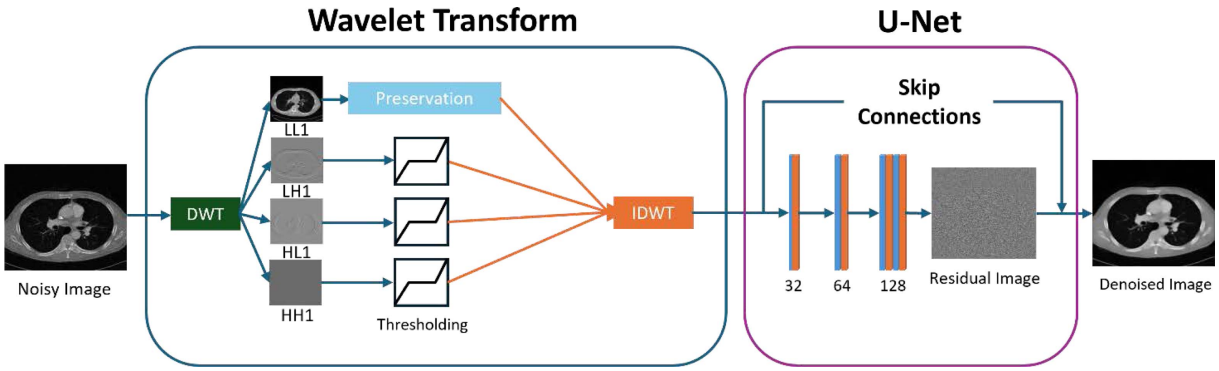

Fig. 3. (Color online) Structural Diagram Representing the Wavelet Transform Process.

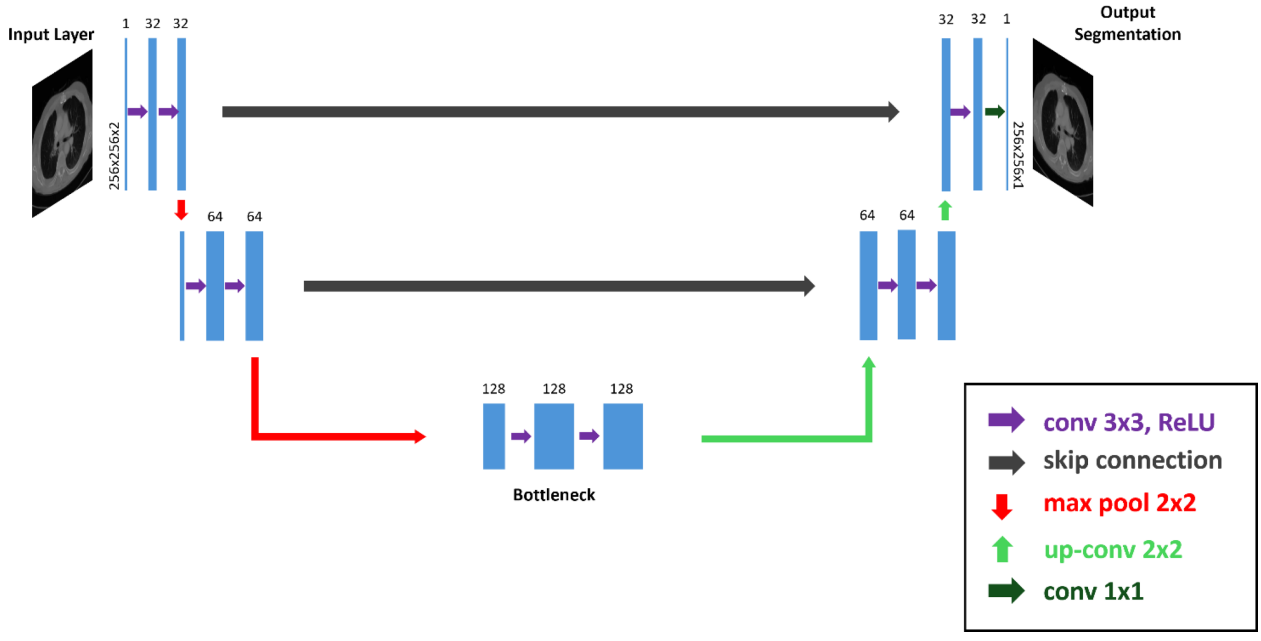

Fig. 4. (Color online) Architecture of the U-Net Model for CT Image Denoising.

layer extracts core information via a 128-channel convolutional layer. The decoding path restores spatial resolution (64 to 32 channels) by integrating low-level features from the encoding path with high-level features from the bottleneck layer via upsampling and skip connections. The final output passes through a 1 × 1 convolutional layer with a sigmoid activation function to generate a single-channel grayscale image for pixel-wise prediction [30, 31].

2.6. Experimental Data and Hyperparameters

The dataset used in this study is a publicly available CT image dataset from Kaggle, consisting of 100 Chest/Abdomen CT DICOM files collected from 100 patients [32]. The entire dataset was split into 80% for training and 20% for validation to train the model. The Structural Similarity Index (SSIM)-based loss function was utilized for model training. This function quantifies the similarity between the original and predicted images by comprehensively considering the image's brightness, contrast, and structure. The main hyperparameters of the model were set as shown in Table 1. The initial learning rate was set to 0.0001, and the batch size was set to 8. The Adaptive Moment Estimation (Adam) algorithm was used as the optimizer. The maximum number of epochs was set to 100, but Early Stopping was implemented to terminate training if the validation loss did not improve for more than 10 consecutive epochs. The Rectified Linear Unit (ReLU) was used as the activation function, and the output layer utilized the sigmoid function to reflect the grayscale characteristics of CT images [33].

Table 1. Main Hyperparameter Settings for Model Training.

Hyperparameter	Value/Setting
Learning rate	0.0001
Batch size	8
Optimizer	Adam
Epoch	100
Activation function	ReLU
Loss function	SSIM Loss

3. Result

In this study, to quantitatively evaluate the CT image noise reduction performance of the proposed Wavelet Transform-based U-Net model, Low-dose CT (LDCT) images were simulated by adjusting the standard deviation of noise (σ) from 0.01 to 0.1 in 0.01 increments. Gaussian noise corresponding to each standard deviation level was randomly added to the CT images with the applied ROI, and the noise reduction performance of each model was compared and analyzed. Performance evaluation was

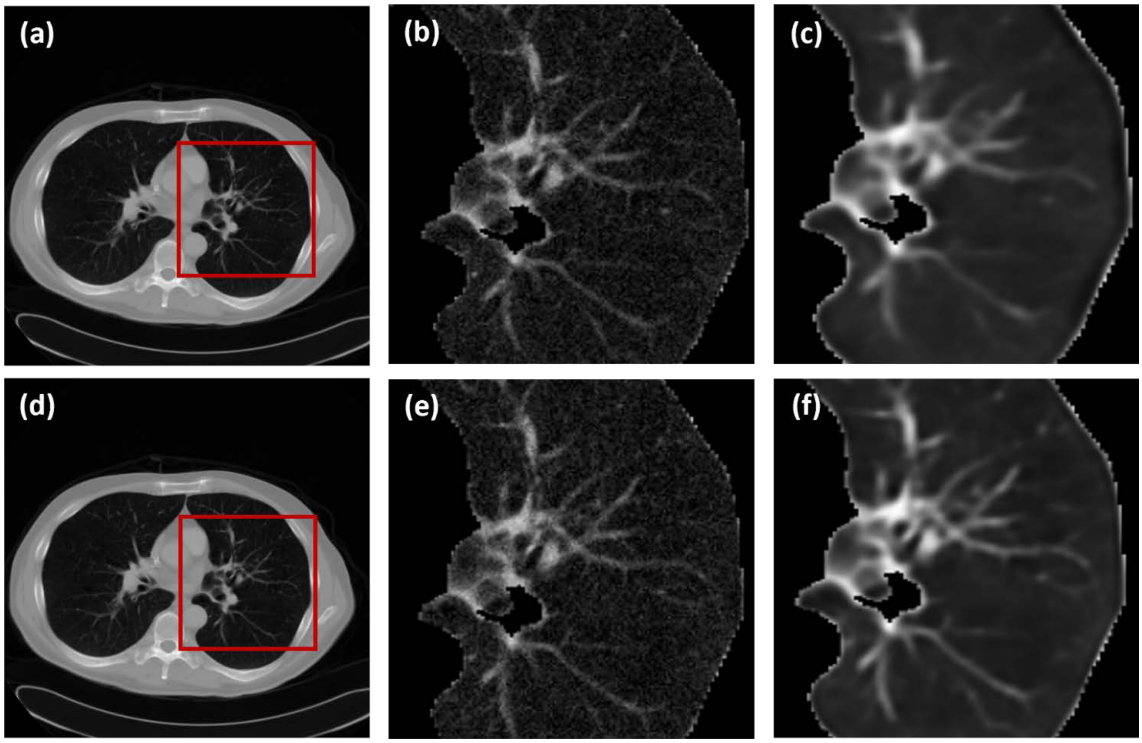

Fig. 5. (Color online) Comparison of CT Image Denoising Results Using U-Net, Wavelet+U-Net.

Table 2. Comparison of PSNR and SSIM Performance at Different Noise Levels Using a Single U-Net Model.

Noise Std	PSNR (Noisy)	PSNR (Denoised)	SSIM (Noisy)	SSIM (Denoised)
0.01	40.0200	35.0228	0.9226	0.9384
0.02	34.0363	33.9059	0.7669	0.9211
0.03	30.5993	32.8385	0.6150	0.9009
0.04	28.2010	32.0766	0.4937	0.8720
0.05	26.3685	30.9997	0.4025	0.8682
0.06	24.8867	30.2699	0.3342	0.8367
0.07	23.6345	29.1445	0.2824	0.8144
0.08	22.5619	28.3559	0.2424	0.7907
0.09	21.6124	27.9725	0.2109	0.7611
0.10	20.7616	26.9915	0.1857	0.7273

Table 3. Comparison of PSNR and SSIM Performance at Different Noise Levels Using the Wavelet-based U-Net Model.

Noise Std	PSNR (Noisy)	PSNR (Denoised)	SSIM (Noisy)	SSIM (Denoised)
0.01	40.0364	35.8833	0.9226	0.9456
0.02	34.0276	34.9215	0.7668	0.9309
0.03	30.6666	33.7251	0.6149	0.9192
0.04	28.3020	33.3109	0.4938	0.8966
0.05	26.4122	32.5639	0.4024	0.8823
0.06	24.8828	32.0505	0.3341	0.8562
0.07	23.5954	31.4289	0.2824	0.8452
0.08	22.5334	30.3017	0.2423	0.8135
0.09	21.4944	30.0518	0.2109	0.7959
0.10	20.7153	29.1712	0.1857	0.7795

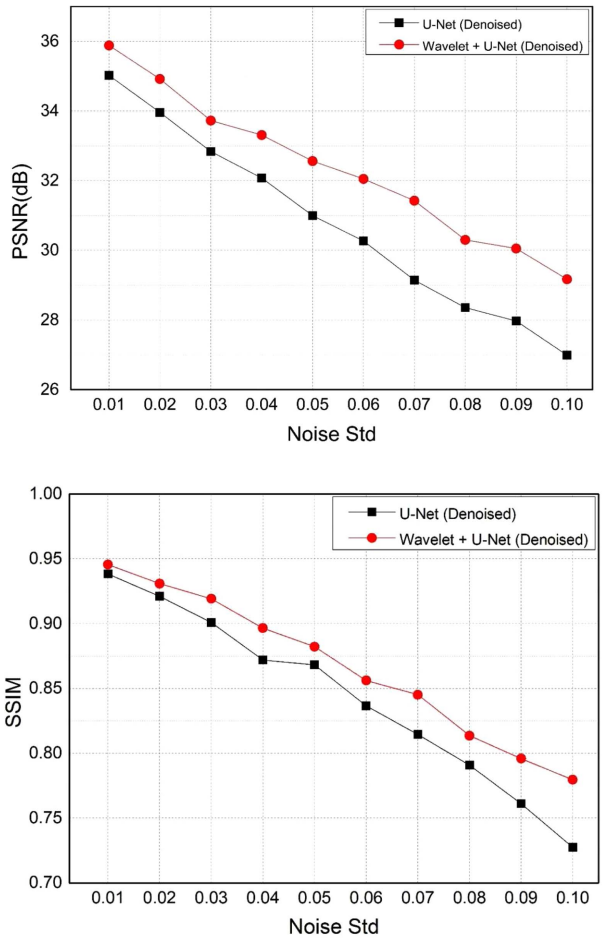

Fig. 6. (Color online) Mean PSNR and SSIM Across Varying Noise Standard Deviations.

carried out by comparing the U-Net model with the Wavelet Transform applied as a preprocessing step against the conventional U-Net model without it. All experimental results were quantitatively analyzed based on mean values. Peak Signal-to-Noise Ratio (PSNR) and Structural Similarity Index (SSIM) were used as image reconstruction performance metrics. Generally, a higher PSNR value indicates superior noise reduction performance, and an SSIM value closer to 1 signifies higher structural similarity between the two images [34]. Fig. 5 shows (a) the reference CT image, (b) the magnified image with noise applied, and (c) the reconstructed result from the U-Net model without the Wavelet Transform. Figures (d), (e), and (f) show the reference CT image, the magnified image with noise applied, and the reconstructed result using the U-Net model with the Wavelet Transform, respectively. Table 2 and Table 3 summarize the PSNR and SSIM values after noise removal for each model, confirming that the proposed Wavelet-based U-Net model generally outperformed the conventional U-Net. Fig. 6 shows the average PSNR and SSIM scores according to the standard deviation of the noise. The Wavelet Transform-integrated U-Net model consistently exhibited higher values in both metrics compared to the standalone conventional U-Net model.

4. Discussion

This study proposed a novel framework that integrates the Wavelet Transform with the U-Net architecture to effectively eliminate noise in CT images and overcome the limitations of conventional deep learning models, namely the loss of fine anatomical structures and blurring artifacts. Recognizing that existing deep learning noise reduction techniques suffer from these drawbacks, we utilized the multi-resolution analysis capability of the Wavelet Transform and an adaptive thresholding scheme in the preprocessing stage. The core factor driving the

performance improvement is the Discrete Wavelet Transform's (DWT) multi-resolution analysis combined with a selective noise reduction strategy. DWT efficiently separates the CT image into a low-frequency component containing structural information and a high-frequency component containing boundary and noise information. In this process, the low-frequency component is preserved to maintain major anatomical structures, while a threshold is applied only to the high-frequency component, where noise is concentrated, to suppress the noise. This pre-processing step effectively and in advance lowers the noise level of the image input to the U-Net. The conventional standalone U-Net model must simultaneously process both noise and meaningful structural information in the input image, inevitably leading to blurring artifacts where boundary and fine texture information is obscured during the noise reduction process. In contrast, the proposed model inputs a noise-reduced image (reconstructed via IDWT) into the U-Net, allowing U-Net to focus more on structural feature restoration rather than complex noise suppression. Consequently, the increase in PSNR quantitatively supports the noise suppression capability, while the enhancement in SSIM confirms the ability to preserve fine structures. This demonstrates that the integration of Wavelet preprocessing effectively addresses the fine detail loss observed in conventional deep learning denoising, marking a significant contribution to high-fidelity CT image reconstruction.

However, this study has the following limitations. First, the Wavelet Transform and thresholding were performed as a fixed preprocessing step, separate from the U-Net's learning process. This hinders end-to-end optimization, where wavelet coefficients could directly contribute to the deep learning model's output, leaving room for further performance improvement. Second, the scaling and correction factors used for threshold setting were determined via an empirical formula. This dependence means that the generalization performance may degrade when applied to various patient datasets or CT systems with different noise distributions. To overcome these limitations, future work plans to introduce a 'learnable wavelet layer' structure, integrating the Wavelet Transform as a part of the deep learning network. This will allow the DWT coefficients to be optimized via backpropagation, enabling more precise capture of image features. Furthermore, we aim to develop a 'data-driven adaptive thresholding module' that automatically learns and adjusts the threshold based on the local noise distribution and structural complexity of the input image, rather than relying on a fixed empirical threshold, thereby enhancing the model's generalization capability. Finally, we will verify the restoration performance against various types of noise and conduct in-depth comparative analysis with other state-of-the-art noise reduction models.

5. Conclusion

This study proposed an optimized framework that combines the Wavelet Transform with U-Net to improve the performance of existing deep learning-based CT image reconstruction. Acknowledging the limitations of deep learning noise reduction methods, such as fine structure loss and blurring, we utilized the multi-resolution analysis of the Wavelet Transform and an adaptive thresholding technique in the preprocessing stage. The essence of the proposed model is the maximization of the U-Net's structural feature restoration capability by using the Discrete Wavelet Transform to decompose the image into low- and high-frequency components and applying selective noise removal only to the high-frequency component where noise is concentrated. Quantitative evaluation confirmed that the proposed Wavelet-based U-Net model consistently showed improved PSNR and SSIM scores across all noise levels compared to the standalone conventional U-Net model. This demonstrates that the framework proposed in this study is excellent at suppressing noise while preserving the image's structural similarity and fine anatomical information. The findings of this research have the significance of substantially contributing to the improvement of CT image quality for clinical applications.

Acknowledgement

This work was supported by Dongseo University 『Dongseo Frontier Project』 Research Fund of 2025.

References

[1] M. Diwakar, M. Kumar, and M. Biomed. Signal Process. Control. **42**, 73 (2018).
[2] N. Saidulu and P. R. Muduli, Comput. Biol. Med. **190**, 109965 (2025).
[3] X. Chen, X. Wang, K. Zhang, K. M. Fung, T. C. Thai, K. Moore, R. S. Mannel, H. Liu, B. Zheng, and Y. Qiu, Med. Image Anal. **79**, 102444 (2022).
[4] K. Kim, C. Park, and Y. Lee, J. Magn. **29**, 237 (2024).
[5] S. J. Kang and A. L. Lee, J. Magn. **24**, 286 (2019).
[6] M. Tsuneki, J. Oral Biosci. **64**, 312 (2022).
[7] O. Ronneberger, P. Fischer, and T. Brox, Med. Image Comput. Comput. Assist. Interv. (MICCAI). **9351**, 234 (2015).

[8] C. Y. Park and B. Jo, J. Magn. **29**, 550 (2024).
[9] E. Kang, J. Min, and J. C. Ye, Med. Phys. **44**, e360 (2017).
[10] H. Chen, Y. Zhang, M. K. Kalra, F. Lin, Y. Chen, P.Liao, J. Zhou, and G. Wang, IEEE Trans. Med. Imaging. **36**, 2524 (2017).
[11] K. Zhang, W. Zuo, Y. Chen, D. Meng, and L. Zhang, IEEE Trans. Image Process. **26**, 3142 (2017).
[12] W. Kim, J. Lee, M. Kang, J. S. Kim, and J. H. Choi, PLoS One **17**, e0274308 (2022).
[13] Y. Zhao, S. Wang, Y. Zhang, S. Qiao, and M. Zhang, Complex Intell. Syst. **9**, 6971 (2023).
[14] G. Litjens, T. Kooi, B. E. Bejnordi, A. A. A. Setio, F. Ciompi, M. Ghafoorian, J. van der Laak, B. van Ginneken, and C. Sánchez, Med. Image Anal. **42**, 60 (2017).
[15] C. Tian, M. Zheng, W. Zuo, B. Zhang, Y. Zhang, and D. Zhang, Pattern Recognit. **134**, 109050 (2023).
[16] W. Dong and H. Ding, Neurocomputing **214**, 902 (2016).
[17] M. S. Priyadarshini, M. Bajaj, L. Prokop, and M. Berhanu, Sci. Rep. **14**, 3443 (2024).
[18] J. Gu, Y. Peng, H. Lu, X. Chang, and G. Chen, Measurement **200**, 111635 (2022).
[19] D. Chen, S. Wan, J. Xiang, and F. S. Bao, PLoS One **12**, e0173138 (2017).
[20] Y. Jang, J. Y. Sim, J.-R. Yang, and N. K. Kwon, Sensors **21**, 1851 (2021).
[21] H. Khorrami and M. Moavenian, Expert Syst. Appl. **37**, 5751 (2010).
[22] M. Mohamed and M. Deriche, Int. J. Comput. Appl. **96**, 36 (2014).
[23] D. Popov, A. Gapochkin, and A. Nekrasov, Electronics. **7**, 120 (2018).
[24] D. L. Donoho, IEEE Trans. Inf. Theory. **41**, 613 (1995).
[25] D. L. Donoho and I. M. Johnstone, J. Am. Stat. Assoc. **90**, 1200 (1995).
[26] S. G. Chang, B. Yu, and M. Vetterli, IEEE Trans. Image Process. **9**, 1532 (2000).
[27] C. Risoli, M. Nicolo, D. Colombi, M. Moia, F. Rapacioli, P. Anselmi, E. Michieletti, R. Ambrosini, M. D. Terlizzi, L. Grazioli, C. Colmo, A. D. Naro, M. P. Natale, A. Tombolesi, A. Adraman, D. Tuttolomondo, C. Costantino, E. Vetti, and C. Martini, Diagnostics (Basel) **12**, 1501 (2022).
[28] J. H. Im, I. J. Lee, Y. Choi, J. Sung, J. S. Ha, and H. Lee, Cancers **14**, 3581 (2022).
[29] J. Wasserthal, H.-C. Breit, M. T. Meyer, M. Pradella, D. Hinck, A. W. Sauter, T. Heye, D. T. Boll, J. Cyriac, S. Yang, M. Bach, and M. Segeroth, Radiol. Artif. Intell. **5**, e230024 (2023).
[30] D. P. Kingma and J. Ba, arXiv preprint arXiv:1412.6980 (2014).
[31] J. Zhang, Y. Niu, Z. Shangguan, W. Gong, and Y. Cheng, Comput. Biol. Med. **152**, 106387 (2023).
[32] K. Clark, B. Vendt, K. Smith, J. Freymann, J. Kirby, P. Koppel, S. Moore, S. Phillips, D. Maffitt, M. Pringle, L. Tarbox, and F. Prior, J. Digit. Imaging. **26**, 1045 (2013).
[33] X. Wang, C. Wu, Y. Lu, and M. Tian, Appl. Sci. **12**, 7031 (2022).
[34] H. Jin, Y. Tang, F. Liao, Q. Du, Z. Wu, M. Li, and J. Zheng, Signal Process. Control. **96**, 106548 (2024).